

# Numerical Simulation of the Compressible and Turbulent Mixing layer Developing Temporarily and Spatially Using the Spectral Element technique

## Milton Biage

School of Mechanical Engineering  
Federal University of Uberlândia, MG-Brazil  
[milton@ufu.br](mailto:milton@ufu.br)

## Paulo Lopes da Silva Junior

School of Mechanical Engineering  
Federal University of Uberlândia, MG-Brazil  
[plopes@mecanica.ufu.br](mailto:plopes@mecanica.ufu.br)

## Luciana Faria Costa

School of Mechanical Engineering  
Federal University of Uberlândia, MG-Brazil

## Cassius Ricardo Nascimento Ferreira

School of Mechanical Engineering  
Federal University of Uberlândia, MG-Brazil  
[Cassius@mecanica.ufu.br](mailto:Cassius@mecanica.ufu.br)

**Abstract.** *The two-dimensional plane shear layers for high Reynolds numbers are simulated using the transient explicit Spectral element Collocation method. The fast and slow air streams are submitted to the different densities. A temporally growing mixing layer, developing from a hyperbolic tangent velocity profile to which is superposed an infinitesimal white-noise perturbation over the initial condition, is studied. In the same way, a spatially growing mixing layer is also study. In this case, the flow in the inlet of the domain is perturbed by a time dependent white noise of small amplitude. For all cases studied, the structure of the vorticity, transversal velocity and the internal energy are visualized for high Reynolds number. One shows that broadband kinetic energy and temperature spectra develop after the first pairing. The results showed that similar conclusions are obtained for the temporal and spatial mixing layer. Particularly, the spreading rate of the layer in very good agreement with the results presented in the literature.*

**Keywords.** Mixing layer, Chebyshev Collocation Spectral Method, Compressible Flow, Stratified Flow.

## 1 Introduction

The intensely turbulent region formed at the boundary between two parallel fluid streams of different velocity has been studied for many years. This kind of flow is called of mixing layer. The mixing layer of a Newtonian fluid, non-reactive and compressible flow, practically, is one of the simplest turbulent flow. However, this flow presents in its structure the most complex behavior existing in turbulent shear flows. The mixing layer characteristics depend the initial and boundary conditions, the Reynolds number and the Mach number.

The most of mixing layer studies in laboratory is the case of mixing layer growing spatially. Nevertheless, in numerical studies the analysis of mixing layer growing temporally is intensely studied, due its implementation in numerical code is easily. In addition, there are very important linear and nonlinear dynamic features that are common to the two flows, so a detailed analysis of numerical simulations of a temporally growing can yield important insight into the evolution in the spatial case.

In the turbulent mixing layer, the coherent large structure takes the form of quasi two-dimensional vortices aligned across the span of the flow. The larger part of the turbulent kinetic energy can be directly associated with these vortices. Vortex interactions are responsible for the cross stream momentum transfer. This fact can be enhanced by the two examples of mixing layer study at a low and high Reynolds numbers, respectively. The study performed by Winant and Browand (1974), at moderate Reynolds numbers, showed that the most visible features of the flow are the compact regions of high vorticity. These vortex structures are aligned across the direction of the flow. The mixing layer grows in thickness as a result of a coalescence of neighboring vortices in a characteristic interaction termed vortex pairing. On the other hand, Brown and Roshko(1974) carried out a mixing layer research at a larger Reynolds numbers. Also, the most prominent feature of the flow is again the large scale structures. The central core regions contain an excess of the fluid vorticity. In these two studies is remarked that the major dynamically feature of the mixing layer to be the

formation and interaction of two-dimensional vortices. The interaction appears to be independent of Reynolds number and it must therefore be inviscid. We would expect the same features and interactions to appear at all Reynolds numbers. There is regularity and a repeatability implied in the observations, which suggest deterministic models, might be more useful than the traditional statistical formulations. The presence of much smaller scales of fluctuation does not appear to destroy the spatial coherence integrity of the large scale vortices. Somehow large scales and small scales coexist in a manner that is not well understood. These two studies with large quantitative visualizations and the others notable results contributed to support this conclusion. Among them, Konrad (1976), Breidenthal (1978), Roshko (1980) and Bernal (1976) who have concentrated their studies on the description of the small scale structure. Dimotakis and Brown (1976) studied the time scales and orientation of the large vortex structures. Jimenez (1980) have noted the onset of smaller scales and paid particular attention to the semi-permanent, three-dimensional structure of these features. He showed that the large structure presents in mixing layer has a self-preserving behavior. In conclusion, the result of several researches showed that the large vortex's structures are not altered when the Reynolds number increases. Augmenting the Reynolds number, the small scale increases too, without change the feature of the large scale.

While the original motivation for this study came from questions as to the behavior of the explicit Spectral Collocation Method to simulate unstable flow at high Reynolds numbers, our attention was also turned to even more fundamental questions about the flow structure at high Reynolds number, of which various facets were revealed that support the principal behavior enhanced by the several researches performed in mixing layer. In particular, one evinces the temperature behavior in the structure flow. One shows that broad-band kinetic energy and temperature spectra develop after the first pairing, having both the same behaviors.

## 2 Mathematical Formulation

In this study we used the laminar compressible flow formulation, considering the fact that the mixing layer structure is basically constituted by large coherent vortices; thus we guess that the large structures are accurately simulated. In addition, we used in this study a fine grid and a numerical filter that has dissipative behavior, causing a representative effect for the small scale of the turbulence (Anderson et al., 1995):

The problem consists by two layers: fast and slow air streams. The origin is located at the downstream edge of the thin splitter plate. The lower air stream has the following dimensional properties: the streamwise velocity  $U_{-\infty}^*$ , temperature  $T_{-\infty}^*$ , total enthalpy  $H_{-\infty}^*$ , density  $\rho_{-\infty}^*$  and zero average transverse velocity, while the upper air stream is likewise characterized by  $U_{\infty}^*$ ,  $T_{\infty}^*$ ,  $H_{\infty}^*$ ,  $\rho_{\infty}^*$  and zero average transverse velocity. The asterisk upper-index represents the dimensional variables and the free-stream flow is denoted by the infinite under-index. The computational domain is rectangular, with  $-L_x^* \leq x \leq L_x^*$  and  $-L_y^* \leq y \leq L_y^*$ .

We applied the adequate characteristic scale parameter upon the two-dimensional averaging governing equations to obtain their dimensionless vectorial form. For this, the following dimensionless groups are used:

$$x = \frac{x^*}{L_x/2}, y = \frac{y^*}{L_y/2}, t = \frac{t^* \bar{U}}{L_x/2}, u = \frac{u^*}{\bar{U}}, v = \frac{v^*}{\bar{U}} \quad (1,2,3,4,5)$$

$$T = \frac{T^*}{\bar{T}}, \rho = \frac{\rho^*}{\bar{\rho}}, P = \frac{P^*}{\bar{\rho} \bar{U}^2}, E = \frac{E^*}{\bar{U}}, \mu = \frac{\mu^*}{\bar{\mu}} \quad (6,7,8,9,10)$$

where  $\mu^*$  is the dynamic viscosity,  $K^*$  is thermal conductivity. The variables  $P^*$ ,  $\rho^*$ ,  $T^*$  and  $E^*$  represent the dimensional pressure, density, temperature and the total energy, respectively and  $u^*$  and  $v^*$  represent the components of the velocity vector. The total energy is defined as:  $E^* = e_i^* + |\vec{V}|^2/2$ , where  $e_i^*$  is the dimensional internal energy.

We also define the following equation

$$\bar{\Pi}_i = \frac{\left(\Pi_{\infty}^*\right)_i + \left(\Pi_{-\infty}^*\right)_i}{2}, \quad \Pi_i = \frac{\left(\Pi_{\infty}^*\right)_i - \left(\Pi_{-\infty}^*\right)_i}{2} \quad \text{with } I=1,2,\dots \quad (11,12)$$

where  $\pi_i$ , with  $I=1,2,3,\dots$ , correspond to all variables described above that one needs to define the average and the difference properties.

We applied the adequate characteristic scale parameter, described by eqns. (1) to (10), upon the two-dimensional conservative governing equations to obtain their dimensionless vectorial form:

$$\frac{\partial w}{\partial t} + \frac{L_y}{L_x} \frac{\partial F}{\partial x} + \frac{\partial G}{\partial y} = 0 \quad (13)$$

where  $w$  is the vector of dependent variables,  $F$  and  $G$  involve the convective and dissipative terms in the  $x$  and  $y$  directions, respectively. We do not write the equation of these terms and the equations of others subsequent definitions (for detail see Anderson et al., 1995). To close the problem, the ideal gas state equation is used. To evaluate the transport properties as a function of the temperature in the domain, we used the Sutherland formula for the viscosity and the thermal conductivity (Whyte, 1974).

In this study of an air mixing layer growing spatially we assume as boundary conditions the hyperbolic-tangent profiles for all fields in the flow upstream and free-slip conditions on the lateral of the computational domain that permit, as simply as possible, unconstrained motion in the  $y$ -direction. In this kind of mixing layer, eddies which form inside the domain have to be evacuated downstream, at  $x=1$ . For this purpose, we have used an outflow boundary condition, based on a radiative Sommerfeld condition, and developed by Orlanski (1976). However, for temporal mixing layer, the axial boundary conditions are different of that ones assumed for spatially mixing layer. Initially, we assume the hyperbolic-tangent profiles in both axial limits, and when the time flows we preserve the periodicity of these conditions in stream flow limits by an iterative numerical procedure. The initial conditions are the same for the two kinds mixing layer studied in this work: temporal and spatial. We assume as initial conditions the hyperbolic-tangent profiles on the all domain.

In mixing layer growing spatially, we applied white noises over the boundary conditions in  $x=-1$ , all time. However, in simulation of mixing layer growing temporally, different from mixing layer growing spatially, we applied the white noise only over the initial condition. White noise will be injected with the same small amount of energy into all the longitudinal modes of the basic flow properties. The energy injected into the stable modes will be damped. On the contrary, any unstable mode (particularly the most amplified one), will grow at its own amplified rate, given by the instability theory. Thus, the most amplified mode emerges from the small chaotic perturbations, due to the instability of the basic profile. The white-noise model, represents in a very approximate way, the residual turbulence that is experimentally responsible for the growth of instabilities. These small values of white-noise are sufficient to induce eddies.

We define the vorticity thickness of the mixing-layer at a given time as

$$\delta(t) = \frac{2U}{\max \left| \frac{\partial \bar{u}}{\partial y} \right|}, \quad \text{where} \quad \bar{u}(y) = \frac{1}{2} \int_{-1}^1 u(x, y, t) dy \quad (14, 15)$$

where  $\delta_0 = 1/2\delta(0)$ .

### 3. Results and Analises

To obtain the results in this study we used an explicit Chebyshev Spectral collocation method (Cannuto et al., 1988). The convenient way to assure a steady state solution independent of the time step is to separate completely the space and time discretization procedures [Jameson, Schmidt and Turkel, 1981]. In this scheme, one begins by applying a semi-discretization over the governing equations (that are given by Eqn. (13), in which only the spatial derivatives are approximated. The resulting ordinary differential equations are then solved by a multi-stage time stepping procedure. In this work was applied the Runge-Kutta method of  $s$ -order, suggested by Jameson, Schimidt e Turkel (1989).

The simulations obtained with aid of a molecular dissipative term are called direct numerical simulation. In the direct numerical simulations, the cutoff scale has to match the two-dimensional dissipative scale. In this case the calculate needs to limit a very limited molecular Reynolds number. Thus, to simulate the large scale field in high Reynolds number, without using a subgrid-scale parametrization, we need to use a filter to stabilize the numerical code. The filtering or smoothing aims to dump the small wavelengths, characterizing the noises introduce by the numerical errors. However, when the filtering procedure is applied, the small scale of the physical problem can also be smoothed. In our work we used the exponential cut-off filter of order four (Cannuto et al., 1988) that permit minimize this fact. In the same way, one needs use a filtering sensor to select the filtering moment and mesh points to smooth. The better sensor that we found for our study was a fixed variation range, which establishes the maximum and minimum variation for all variables. Generally, the unstable variables caused by numerical errors present their values significantly different

in comparison with the values the same variables in the mesh neighboring points. Thus, if these discontinuities extrapolate the limits established by the sensor, the filter is applied over the variable in question, in the all domain.

The ideal domain dimensions to simulate mixing layers have to contain an integer number of fundamental eddies (the dimensional periodicity of the fundamental wavelength is  $\lambda_a \approx 14.13\delta_0$ , as suggested in the literature), according to  $L_i^* = m_i \lambda_a$ , with  $i=x$  and  $y$ , where  $m_i$  is the number of the fundamental eddies fixed to the direction  $i$  (Comte et al., 1989). This establishment is relevant because one sets, in advance, the behavior of the flow structure. For the simulation the spatial mixing layer problem, it was setup  $m_y = 1/2 m_x$ , thus, it is imposed in advance the periodicity in the  $x$ -direction, without to block the lateral spreading of the layer before any long period of mixing layer growing. However, it was fixed  $m_y = m_x$  to perform the simulation about the temporal mixing layer, because the temporal mixing layer the lateral spreading is larger, facilitating to observe in the layer, a complete development cycle, involving the pairing mechanisms and rotation and the coalescence process, until that is reduced the group of vortexes to an only one.

The mesh of the computational domain was obtained, locating  $N_x$  and  $N_y$  Chebyshev-Gauss-Lobatto points for each elements, in the directions  $x$  and  $y$ , respectively. In this study it was fixed  $N_x = 30$  e  $N_y = 30$ , however, using  $Ne_x = 30$  and  $Ne_y = 30$  (where  $Ne_x$  and  $Ne_y$  are the numbers of elements in the directions  $x$  and  $y$ , respectively). Assuming that the dependent variables are known at each point from the initial conditions, a system of ordinary differential equations is obtained separately to each point. The flux  $F$  and  $G$  in the Eqn. (13) involve both the terms convective and diffusive, in the directions  $x$  and  $y$ , respectively. These fluxes are approached for each point. The numerical estimate of the fluxes  $F$  and  $G$ , however, need an approximation of the first partial derivatives for the velocity and temperature to evaluate the shear stress and heat flux components. We used the Rapid Chebyshev Transform to obtain these derivatives. This Code is an efficient and rapid manner to obtain the derivatives of first order, as characterized by Cannuto et al. (1988). In same way, we have used this Code to evaluate the derivatives of the Fluxes  $F$  and  $G$ , in Eqn. (13).

We have performed high-resolution (900x900 mode) simulations of a fully turbulent mixing layer, and it is instructive to relate the evolution of these flows to the class of instabilities discussed so far. However, the elements presented dimensions differentiated in the direction  $y$ , where the smallest element locates in the center of the layer, while the largest ones locate close of the lateral borders of the domain. A relationship of four was maintained between the largest elements and the smallest element, and this relationship decreases gradually to the moved away of the center elements, in agreement with the following relationship:

$$Y_j = \begin{cases} \frac{2^{ml} \left( \frac{2j - ne_y}{ne_y} \right) - 1}{2^{ml} - 1}, & \text{for } j = \left( \frac{ne_y}{2} + 1 \right) \dots ne_y; \\ -Y_{(ne_y - j + 1)} & \text{for } j = 0 \dots \frac{ne_y}{2}; \end{cases} \quad (16)$$

and

$$y_{ji} = (Y_{j+1} - Y_j) \frac{-\cos\left(\frac{i\pi}{Np}\right) + 1}{2} + Y_j, \quad \text{for } i = 0, \dots, Np \text{ and } j = 0, \dots, Ne_y \quad (17)$$

where  $ml$  is the factor that represents as the mesh will be refined in the center,  $Y$  is a vector that contains the coordinates of the initial point and of the final point for each element,  $Np$  is the number of points contained in each element, the index  $i$  is linked to a point inside of the element, the index  $j$  is linked to the element and finally, the coordinate of the collocation point in the direction  $y$  is  $y_{ji}$ , which represents the coordinate of the point  $i$ , in the element  $j$ .

The results presented on the Figs. 1 was simulated on a computational domain sufficiently large to allow six complete pairings ( $m_x=12$  and  $m_y=12$ ). Spanwise vorticity field presented on Fig. 1 illustrates clear evidence of large scale structures. In this figure are showed the vorticity evolution of mixing layer growing temporally at Reynolds number of 1007, with a velocity ratio,  $\eta_v = U/\bar{U}$ , of  $\infty$  and a temperature ratio,  $\eta_T = T/\bar{T}$ , of 0,2. The plots at eight different times indicate a strong coherence of the vortices, almost regularly spaced.

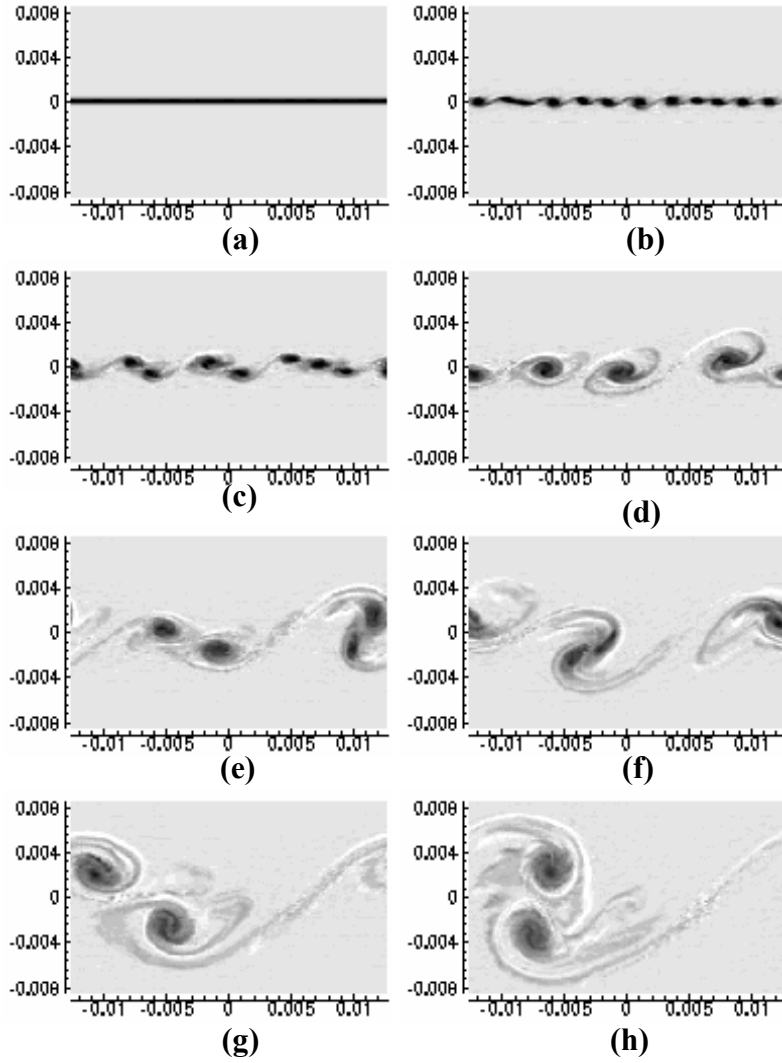


Figure 1: Flow internal vorticity structures evolution,, in temporal mixing layer ( $Re_\infty = 1007$ ,  $M_\infty = 0,26$ ,  $Pr_\infty = 0,72$ ,  $\eta_v = \infty$  e  $\eta_T = 0,2$ ). (a)  $t^* = 0,6389 \times 10^{-2}$  sec.; (b)  $t^* = 1,277 \times 10^{-2}$  sec.; (c)  $t^* = 1,913 \times 10^{-2}$  sec.; (d)  $t^* = 2,549 \times 10^{-2}$  sec.; (e)  $t^* = 3,188 \times 10^{-2}$  sec.; (f)  $t^* = 3,827 \times 10^{-2}$  sec.; (g)  $t^* = 4,466 \times 10^{-2}$  sec.; (h)  $t^* = 5,088 \times 10^{-2}$  sec.;

On the Fig. 1 can also be remarked that the vorticity field is characterized by a straight rotational band of thickness  $\delta_0$ , where the vorticity keeps a negative constant sign. Then, this band widens and begins to oscillate at the wavelength corresponding to the most amplified mode (Fig. 1.b). When the amplitude of the most amplified mode is sufficiently high, the non-linear interactions begin to play a role. This fact corresponds to the situation where the fluid of velocity  $U_\infty^*$  roll-up around the fluid of velocity  $U_{-\infty}^*$ , and conversely, as described in Comte et al. (1989). Thus, a row of Kelvin-Helmholts eddies forms at  $t^* \approx 0.0638$  seconds, as showed on the Fig. 1.b. There, the distance of the vortical core being approximately equal to the fundamental wavelength,  $\lambda_a$ , since these eddies result from the roll-up of a rotational zone of thickness  $\delta_0$ . In this way, one notices that the coherent structures resulting the rotational process of pairing vortex have their diameter approximately equal to  $2\delta_0$ . In our study, this process began by formation 12 vortices (as can be seen in the Figure 2 showing the evolution of the transversal velocity), where in this calculation  $\delta^*(0) = 0.0666$  m,  $\delta_0^* = 1/2\delta^*(0)$ ). As one can be seen on the Figure 2, there are some of them that are smaller, charactering an amplification of a fundamental vortex, slightly different from that one set in advance (the set fundamental wavelength is  $\lambda_a \approx 14.13\delta_0$ ). It can observed on Fig. 1.b that these smaller vortices are to pairing in more two vortex and to rotate more quickly than the other pairing formed, seeming a defined mechanism to reduces the amount of vortices to a pair number and multiple for two to yield four structures of wavelength  $2\lambda_a$ . The vortices remained have delayed pairings. The vortices resulting of the process pairing and coalesce continue their courses of pairing, rotation and coalescence with others, forming pairing with the vortex positioned in its right, as one can observed on the Figure (1.c) to (1.f). This mechanism continues until the number of vortices reduces to one. Different as found by Comte et al. (1989), in the final process, the one resulting vortex continuous to grow until the domain edge compress its evolution. This fact is consistent with theory of mixing layer growing temporally, because of the temporal growing of a vortex represent a behavior of mixing layer growing spatially, at position given by  $x^* = (\partial\delta_i^*/\partial t^*)t^*$ .

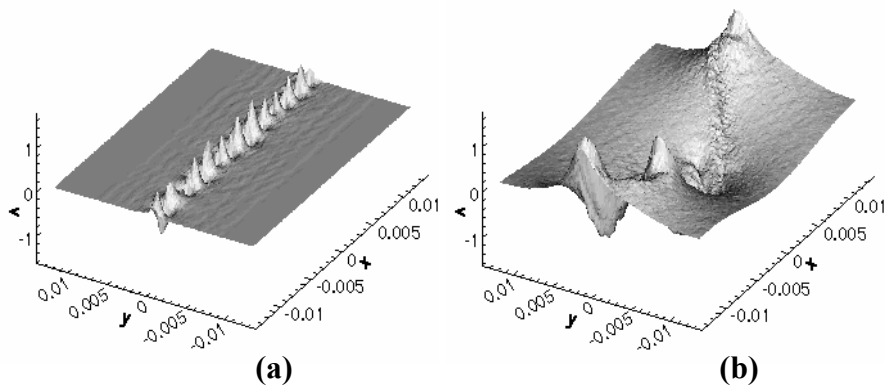


Figure 2: Transverse velocity evolution in the domain, in temporal mixing layer ( $Re_\infty = 1007$ ,  $M_\infty = 0,26$  e  $Pr_\infty = 0,72$ ,  $\eta_v = \infty$  e  $\eta_T = 0,2$ ). (a)  $t^* = 0,6389 \times 10^{-2}$  sec.; (g)  $t^* = 4,466 \times 10^{-2}$  sec).

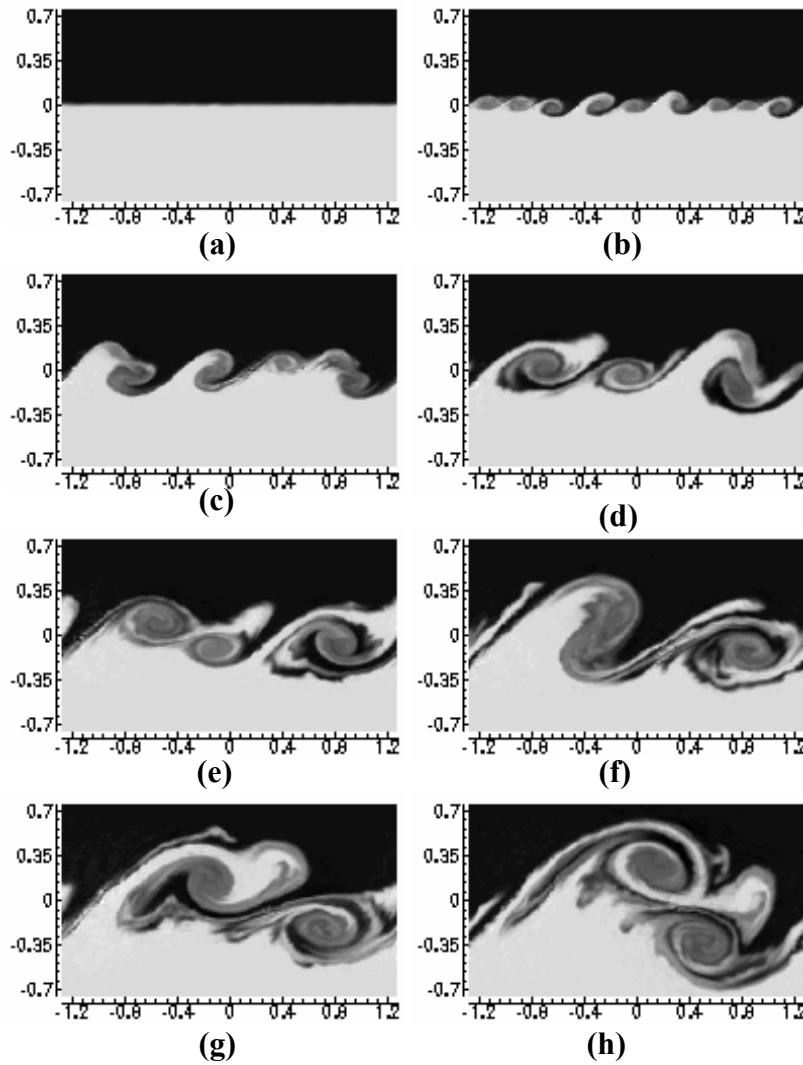


Figure 3: Flow density structures evolution,, in temporal mixing layer. ( $Re_\infty = 1,0 \times 10^5$ ,  $M_\infty = 0,26$ ,  $Pr_\infty = 0,72$ ,  $\eta_v = \infty$  e  $\eta_T = 0,2$ ). (a)  $t^* = 0,6389 \times 10^{-2}$  sec.; (b)  $t^* = 1,277 \times 10^{-2}$  sec.; (c)  $t^* = 1,913 \times 10^{-2}$  sec.; (d)  $t^* = 2,549 \times 10^{-2}$  sec.; (e)  $t^* = 3,188 \times 10^{-2}$  sec.; (f)  $t^* = 3,827 \times 10^{-2}$  sec.; (g)  $t^* = 4,466 \times 10^{-2}$  sec.; (h)  $t^* = 5,088 \times 10^{-2}$  sec.;

Fig.2 shows the transverse velocity for a mixing layer growing temporally, for the same conditions of numerical simulations of the Figs. (1), in two different times: )  $t^* = 0,6389 \times 10^{-2}$  seconds and  $t^* = 4,466 \times 10^{-2}$  seconds. This figure illustrates the coalescence process of the vortices, which occurs in irregular form. In fig. (2.a) is remarked the presence of regular vortices, that correspond to the typically Kelvin-Helmholts eddies, as one can see on the Figs. (1.b). However, the coalescence and rotational processes become more irregular when the time increasing, caused by the delayed pairing process developed for each eddy couple (Fig. (2.b)). We guess that this irregular pairing evolution occurs, essentially, because of the interactions of the stratified flow conditions.

The conclusions presented above could be obtained from Fig. (3), for the internal energy evolution. In this figure are showed the internal energy evolution of mixing layer growing temporally at  $Re_\infty = 1,0 \times 10^5$ , with a velocity ratio,  $\eta_v = U/\bar{U}$ , of  $\infty$  and a temperature ratio,  $\eta_T = T/\bar{T}$ , of 0,2. The plots at eight different times indicate a strong coherence of the vortices, almost regularly spaced, in the same way that observed for the vorticity evolution presented on the Figure (1), although the Reynolds number for the case study in the Figure (3) is considerable higher. Thus one can suggests that the Reynolds number influence fewer the flow structures. Also, there is a remarkable correlation between the vortical and thermal cores, in spite it was not presented illustrations to enhance this fact.

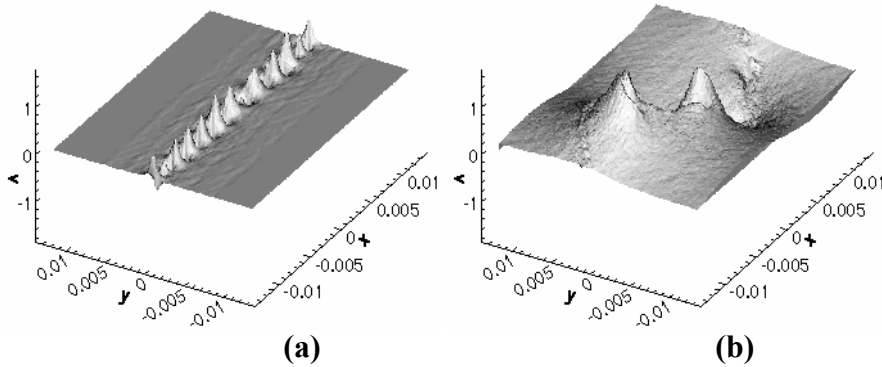


Figura 4: Transverse velocity evolution in the domain, in temporal mixing layer. ( $Re_\infty = 1,0 \times 10^5$ ,  $M_\infty = 0,26$  e  $Pr_\infty = 0,72$ ,  $\eta_v = \infty$  e  $\eta_T = 0,2$ ). (a)  $t^* = 0,01277$  sec.; e (b)  $t^* = 0,04466$  sec).

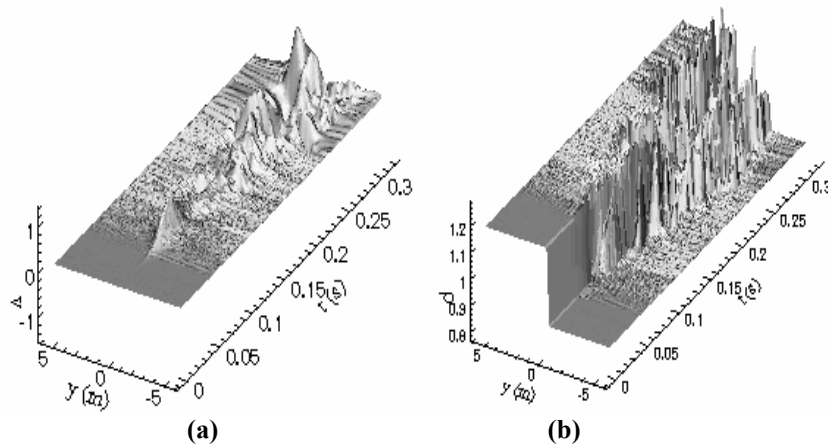


Figure 5: Time evolution of temporal mixing layer, at the station  $x = 2/3 \bullet L_x$ . ( $Re_\infty = 1,0 \times 10^5$ ,  $M_\infty = 0,26$  e  $Pr_\infty = 0,72$ ,  $\eta_v = \infty$  e  $\eta_T = 0,2$ ). (a)  $t^* = 0,01277$  sec.; e (b)  $t^* = 0,04466$  sec). (a) Transverse velocity evolution and (b) Density evolution.

Fig. (4) shows the transverse velocity for a mixing layer growing temporally, for the same conditions of numerical simulations of the Figs. (3), in two different times:  $t^* = 0,01277$  seconds and  $t^* = 0,04466$  seconds. This figure illustrates the coalescence process of the vortices, which occurs in irregular form, completely similar, as shown by Fig. (2) for  $Re_\infty = 1007$ . These results prove more one time that the Reynolds number influences fewer in the flow structure in mixing layer developing temporally. Fig. (5) shows the time evolution of mixing layer growing temporally, at the station  $x = 2/3 \bullet L_x$ , in the same conditions of numerical simulation of figure (3). Evolution of mixing layer growing temporally, along the time at one defined station, give a similar behavior of mixing layer developing spatially. Fig. (5.a) presents the transverse velocity evolution on that one can check the relevance of the temporal approximation, observing similar feature to the spatial approximation. We explore this figure only to enhance this fact. On the Fig. (5.b), it can observe the time density evolution. The use of stratified flow in the study of the mixing layer made in it possible to make some observations of the processes of mixing that are not revealed when the flow there is no change in the density. It is known that the fluid on one side of the mixing layer makes deep incursions into the other side. This is could be confirmed in the study of Brown and Roshko (1974) in that the mixing region shows fluctuation of density

almost equal to the density difference. This fact is closely related to the process of turbulent mixing in the phenomena of entrainment; e.g., the rate of ingestion of non-turbulent fluids into the turbulent region. The entrainment process is associated with the propagation of the turbulent interface into the non-turbulent fluid. This process appears to occur primarily in the formation of the large coherent eddies, interfering in the evolution pairing process, where the non-linear interactions begin to play a role. This description is typically that one showed on the Fig. 5b.

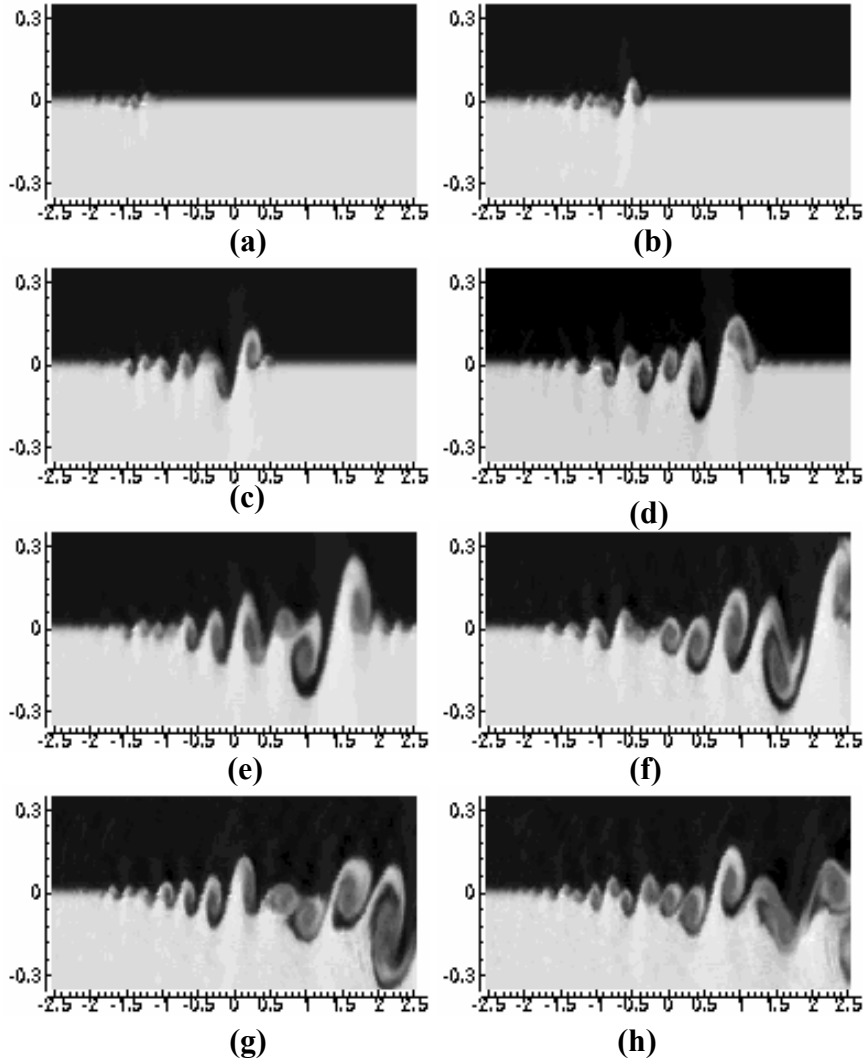


Figure 6: Internal energy structure evolution in spatial mixing layer . ( $Re_\infty = 1.0 \times 10^5$ ,  $M_\infty = 0.26$ ,  $Pr_\infty = 0.72$ ,  $\eta_v = 0.5$  e  $\eta_T = 0.2$ ). (a)  $t^* = 0,0255$  sec.; (b)  $t^* = 0,0383$  sec.; (c)  $t^* = 0,0511$  sec.; (d)  $t^* = 0,0638$  sec.; (e)  $t^* = 0,0765$  sec.; (f)  $t^* = 0,0892$  sec.; (g)  $t^* = 0,1020$  sec.; (h)  $t^* = 0,1148$  sec.).

The results presented on the Figs. 6 and 7 were simulated on a computational domain sufficiently large to allow the evolution the spatial mixing layer. Spanwise internal energy field presented on Fig. 6 and spanwise transversal velocity field showed on Fig. 7 illustrate clear evidence of large scale structures in spatial mixing layer. In these figures are showed the spatial internal energy and transversal velocity evolution at Reynolds number of 100,000, with a velocity ratio of 0.5 and a temperature ratio of 0.28. Some of the description about the pairing vortices and the coalescence process presented above for temporal mixing layer prevail for the spatial mixing layer, as one can see on the Figs. 6 and 7. However, in the spatial approximation studied, the pairing process appears to be more regular. We guess that this fact occurs in consequence of the convective effect, which causes the vortex evacuations. Thus, the pairing and coalescence processes occur with less interference in the space between two successive events. In particular, one remarks on the Figs. 6 and 7 that in spatial mixing layer occurs two kinds of instabilities: absolute and convective. The absolute instability is typically of the temporal mixing layer that occurs in spatial mixing layer in the initial process, caused either by the numerical noise introduced or by the inflectional velocity profile assumed in the initial condition, which is typically for study temporal mixing layer. In posterior process the convective instability Leads the pairing and amalgamation processes.

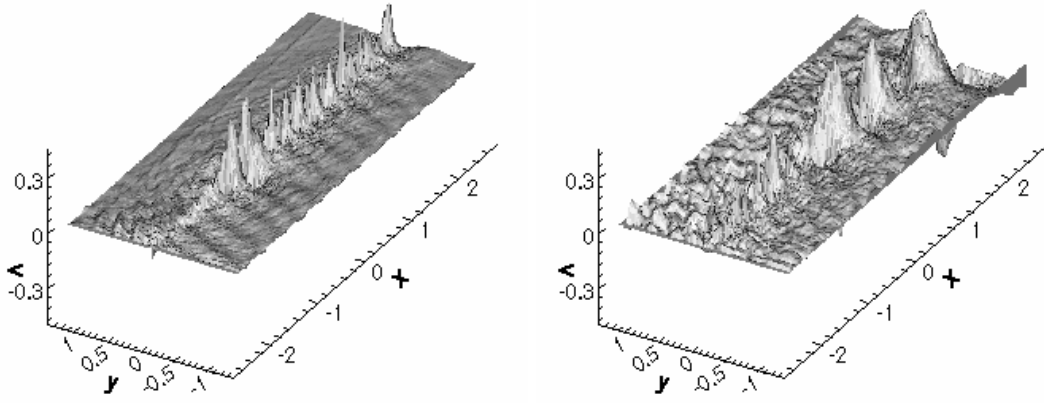


Figure 7: Transverse velocity structure evolution in spatial mixing layer. ( $Re_\infty = 1.0 \times 10^5$ ,  $M_\infty = 0.26$ ,  $Pr_\infty = 0.72$ ,  $\eta_v = 0.5$  e  $\eta_T = 0.2$ ). (a)  $t^* = 0.0383$  sec. (b)  $t^* = 0.102$  sec.

In turbulent mixing layer growing spatially the spacing among the vortices increases when increasing the distance downstream. The eddy diameter also increases. It is expected in spatial approximation that the frequency with which eddies pass any  $x$  stations must be invariant, but on the other hand, the requirement of increasing spacing requires a decreasing frequency. As explained in Brown and Roshko (1974), the lump of vorticity that is an eddy cannot simply disappear, thus it is concluded that, as they convect downstream, eddies must amalgamate in some way into larger structures, and this process must continually recur when increasing  $x$ . The process of amalgamation is related in some way to the process of pairing vortices, in which the tandem arrangement of two successive vortices becomes unstable, and they rotate around each other briefly and become one, the new structure then convecting downstream until the next encounter. Fig. 7 shows the transverse velocity evolution in the domain, in spatial mixing layer, for two different times. The flow aspect described above can be remarked with detail on this figure.

We have calculated (a) one-dimensional longitudinal spatial temperature and (b) kinetic energy spectra, average on the vorticity thickness. These spectra are calculated applying the Rapid Fourier Transform over the numerical results for dimensionless temperature and kinetic energy (defined as  $k = 1/2|\bar{v}|^2$ , where  $\bar{v}$  is the velocity vector), at a given transverse position  $y$  and instant  $t$  as:

$$\Re(k_x, y_i, t_k) = \frac{1}{2} \int_{-1}^1 \xi(x, y_i, t_k) e^{-ik_x x} dx \quad \text{with } i = 0, 1, \dots, N_y \text{ and } k = 1, 2, \dots \quad (18)$$

where  $\Re(k_x, y_i, t_k)$  is the Fourier transform for a given data  $\xi(x, y_i, t_k)$ , temperature or kinetic energy, in a defined transverse direction  $y_i$ , for a given time  $t_k$  and  $k_x$  is the local wavenumber.

The average spectra are obtained integrating the results from the Equation (17) on the thickness vorticity as:

$$E_0(k_x, t_k) = \frac{1}{2} \int_{-\delta(t)/2}^{\delta(t)/2} |\Re(k_x, y_i, t_k)|^2 dy \quad \text{with } k = 0, 1, \dots \quad (19)$$

The dimensionless thermal and kinetic energy spectra are shown on the Figs. 8a and 8b, respectively as a function of the dimensionless wavenumber, for several times, including the completely developed mixing layer. The calculation of these energy spectra using dimensionless properties affects nothing the spectrum feature. These results were obtained from the calculation for mixing layer growing temporally at Reynolds number of 100,000, with a velocity ratio  $\eta_v = 0.5$  and with a temperature ratio  $\eta_T = 0.285$  (similar results presented on Fig. 3 and 4).

As can be seen on these figures the thermal and the kinetic energy inertial ranges extend over a same wavenumber range. This fact is different of that one found by Comte et al. (1989), where they found out that the thermal inertial range extends over a wider wavenumber range than the velocity. They argued in their paper that it occurs due to the

fact of the temperature thickness is larger than the vorticity thickness. In our study, also, this did not occur and the vorticity, temperature and velocity thicknesses have the same amplitude, although the Prandtl number in the two studies was different (in our study it was 0.7 and in their study it was 1). We guess that the Prandtl number only establishes the diffusiveness ratio between velocity and temperature, without interfere in the final distribution of the fields in the mixing layer, after it achieves the completely developed. We noticed that occurs strong interactions between the temperature and velocity fields in mixing layer completely developed, thus these fields will be correlated. This fact is one more consistent fact and a strong coherence between the fields must be expected. One also observes in the thermal and kinetic energy spectra of the mixing layer, displayed in Fig. 8, that both temperature and kinetic energies follow a  $k_x^{-4}$ , completely close to the  $k_x^{-11/3}$ , in the same range, according to the inverse kinetic energy cascade of two-dimensional isotropic turbulence. It enhances the correlated character present in the thermal and momentum fields. This fact is another discordance between our work and the Comte et al. (1989). They have obtained a  $k_x^{-5/3}$  for the thermal energy spectra.

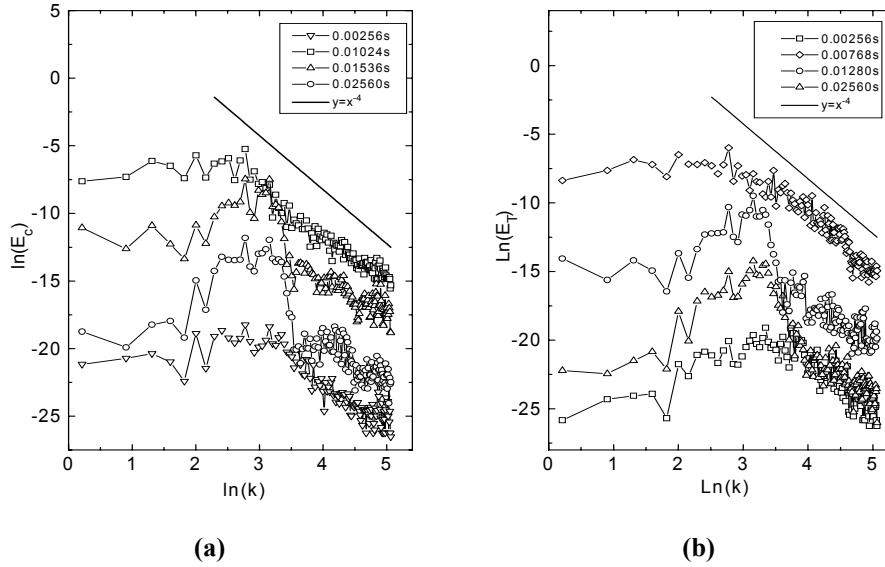


Figure 8: Mixing layer spectra in a mixing layer growing temporally ( $Re_\infty=1.0 \times 10^5$ ,  $M=0.26$ ,  $Pr = 0.72$ ,  $\eta_v = 0.5$  e  $\eta_T = 0.2$ ). (a) Thermal energy spectra for several times and (b) Kinetic energy spectra for several times.

#### 4. Conclusion

Two-dimensional spatial and temporal mixing layers at high Reynolds number have been studied, using the explicit Chebyshev Spectral Collocation Methods. We have analyzed the results, plotting several charts of the internal energy and vorticity fields, and surface of the transverse velocity and density fields, at different times for the two cases of mixing layer studied: spatial and temporal. In particular, we plot the temperature and kinetic energy spectra. In temporal growing mixing layer, we have interpreted the pairing and coalescence process of the coherent vortices. The one-dimensional temperature and kinetic energy spectra show continuo ranges with slopes in agreement with two-dimensional turbulence theory. We have shown that the pairing and coalescence processes occur in a mechanism not completely uniform, where some couple of vortices performed delayed processes between them. One observe that even high Reynolds number the coherent structures are similar that ones present in laminar mixing layer.

#### 5. References

- Anderson, J. D. R., *Computational fluid dynamics*, , McGraw-Hill, New-York 1995
- Bernal, L. P., The coherent structure of turbulent mixing-layers: I. Similarity of the primary vortex structure, II. Secondary streamwise vortex structure, *CAITECH Report*, 1981.
- Breidenthal, R. E., A chemically reacting turbulent shear layer, *Ph. D. Thesis*, California Institute of Technology, 1978.
- Brown, G. L. & Roshko, A., On density effects and large structures in turbulent mixing layers. *J. Fluid Mech.*, 64, pp. 775-816, 1974.
- Canuto, C., Hussaini, M. Y., Quarteroni, A. and Zang, T. A., *Spectral methods in fluid dynamics*, Springer-Verlag, New York, 1988.

- Comte, P., Lesieur, M., Laroche, H. and Normand, X., Numerical simulations of turbulent plane shear layers, *Springer-Verlag*, Berlin Heidelberg, pp. 360-380, 1989.
- Dimotakis, P. And Brown, G. L., The mixing layer at high Reynolds number: Large-structure dynamics and entrainment, *J. Fluid Mech.*, 78, pp. 535-560, 1976.
- Jameson, A., Schimidt, H. and Turkel, E., Numerical solutions of the Euler equation by finite volume methods using Runge-Kutta time stepping schemes, *AIAA Pap. 81-1259*.
- Jimenez, J., On the visual growth of a turbulent mixing layer, *J. Fluid Mech.*, 96, pp. 447-460, 1980.
- Konrad, J. H., An experimental investigation of mixing in two-dimensional turbulent shear flow with applications to diffusion-limited chemical reactions, *Project SQUID Report CIT-8-PU*, 1976.
- Orlanski, I., A simple boundary condition for unbounded hyperbolic flows, *J. Comp. Phys.*, 21, pp. 251-269, 1976.
- Roshko, A., *The plane mixing layer flow visualization results and three-dimensional effects*, Lectures Notes in Physics Springer Pub. Co., 1980.
- White, F. M., *Viscous fluid flow*, McGraw-Hill, New-York, 1974.
- Winant, C. D. & Browand, F. K., Vortex pairing: the mechanism of turbulent mixing-layer growth at moderate Reynolds number, *J. Fluid Mech.*, 63, pp. 237-255, 1974.